

# Co-based Superalloy (Stellite 6) Powder with Added Nanoparticles to be Molten by PTA

Danielle Bond<sup>1</sup> , Rosineide Junkes Lussoli<sup>2</sup>, João Batista Rodrigues Neto<sup>3</sup> , Ana Sofia Clímaco Monteiro D'Oliveira<sup>4</sup> 

<sup>1</sup> Universidade do Estado de Santa Catarina – UDESC, Departamento de Engenharia de Produção e Sistemas, Joinville, SC, Brasil.

<sup>2</sup> Universidade Sociedade Educacional de Santa Catarina – UNISOCIESC, Departamento de Engenharia Mecânica, Joinville, SC, Brasil.

<sup>3</sup> Universidade Federal de Santa Catarina – UFSC, Departamento de Engenharias, Blumenau, SC, Brasil.

<sup>4</sup> Universidade Federal do Paraná – UFPR, Departamento de Engenharia Mecânica, Curitiba, PR, Brasil.

**Como citar:** Bond D, Lussoli RJ, Rodrigues Neto JB, D'Oliveira ASCM. Co-based superalloy (Stellite 6) powder with added nanoparticles to be molten by PTA. *Soldagem & Inspeção*. 2020;25:e2514. <https://doi.org/10.1590/0104-9224/SI25.14>

**Abstract:** Nanotechnology is the domain of technological development and application of materials which go from 1 to 100 nm in at least one of their dimensions. The use of nanoparticles in engineering focuses on the development of new materials with special properties, which can be used as filler materials in the welding field. In this context, this study contributes to the stage preceding the deposition of the weld beads. This work aims to insert, using the colloidal processing technique, ceramic nanoparticles ( $ZrO_2$ ) into a Co-based superalloy (Stellite 6) and study the solidification of this “nanocomposite”. 4 filler materials in the shape of compacted cylinders were melted by PTA: Stellite 6 with added Fe carriers with ceramic nanoparticles ( $ZrO_2$ ) (1%, 2.5% and 7.5% volume) and Stellite 6 without any additions. The molten materials were characterized through optical and scanning electron microscopy with field emission (SEM-FEG), XRD and Vickers microhardness. The results show that the colloidal processing technique was effective in adhering the  $ZrO_2$  nanoparticles to the carrier Fe particles, which were mixed with Stellite 6, as well as the relationship between microstructure refinement, phases and microhardness after PTA melting.

**Key-words:** Nanoparticle carriers; Welding; Superalloys; Solidification; CoCrWC alloy.

## 1. Introduction

Nanotechnology is a multidisciplinary domain involving areas from engineering, physics, chemistry, electronics and biology in the study, technological development and application of materials which go from 1 to 100 nm in at least one of their dimensions [1,2]. Nanoparticles (NPs) are, then, considered to be the substances that have one or more dimensions up to 100 nm, which may have an amorphous or crystalline structure, and may be spherical, tubular or irregularly shaped [3,4]. The use of nanoparticles is already a consolidated reality in some areas, even found in products that go beyond the laboratory and reach the end consumer, such as in the manufacture of paints, which employs  $TiO_2$  nanoparticles, and in the production of sunscreen, which uses ZnO as well. They are still being studied and developed in other areas, with potential application in the cosmetics and textile industries, in medicine, with the drug delivery and gene therapy techniques, in the environmental area, with the possibility of neutralizing soil and water pollutants, and even in the production of industrial lubricants [2].

Nanoparticles can also be employed in Engineering. The development of nanocomposites, nanoparticle-reinforced materials, can be carried out through several processes. Moreno [5] and Vieira et al. [6] present colloidal processing as a possibility. Such processing is widely used to obtain ceramic components, which start from preparing a stabilized suspension (solid + liquid + dispersing agents) with high fluidity, to be poured into plaster molds [7]. Tape casting is another technique used to manufacture nanocomposites, according to [8], aiming at thin flat pieces. Both processes start from a mixture of powders, a dispersant and a solvent, and the nanocomposite is determined by the constitution of such powders and how they are manipulated. The main environmental and industrial advantage of such system is the ability to obtain the suspension using aqueous liquid, even considering metallic powders as a solid phase [9]. The insertion of nanoparticles in composites by casting processes, such as [10], which added nano- $B_4C$  in  $B_4C/Al$  composites by ultrasonic stirring casting, is also noteworthy.

Nanocomposites are also being developed in welding processes such as: TIG (tungsten inert gas), coated electrodes, tubular wires, PTA (plasma transferred arc) and laser. PTA is a welding process in which the powder filler material is introduced into the plasma to form the molten pool with the substrate. The powder is carried by an inert gas (argon) from the powder reservoir to the torch where it will be melted. The energy used to melt the powder comes from the forced passage of the plasma gas (argon) through a water-cooled nozzle, which has a constricting orifice at its end. To start the process, a non-transferred arc, called a pilot arc, is required (the piece is not involved). It is formed between the tungsten electrode (cathode) and the torch's internal copper nozzle (anode). The pilot arc initiates and stabilizes the main arc, and it is extinguished as soon as the main arc is formed [11]. It is noteworthy that, as PTA uses powder filler materials, it allows great flexibility of materials that can be mixed

Recebido: 29 Ago., 2019. Aceito: 30 Mar. 2020.

E-mails: danielle.bond@udesc.br (DB), rosineide.lussoli@unisociesc.com.br (RIL), jbrn.ufsc@gmail.com (JBRN), sofmat.ufpr@gmail.com (ASCMO)



This is an Open Access article distributed under the terms of the Creative Commons Attribution Non-Commercial License which permits unrestricted non-commercial use, distribution, and reproduction in any medium provided the original work is properly cited.

and deposited (including the insertion of carbides and nanoparticles). Several materials, including the superalloys, can be deposited. Nickel-based superalloys are known for their excellent high-temperature corrosion resistance; cobalt-based ones, besides that characteristic, are also very resistant to wearing, with the superalloy commercially known as Stellite 6 being the best known and most used. It has excellent resistance to various forms of chemical and mechanical degradation under temperature and maintains its hardness up to 500 °C. Used in many hardfacing processes, it has a low tendency to crack when compared to other alloys in the Co-Cr-W-C system, since its C content (1.2%) generally tends to produce hypoeutectic microstructures [12].

Besides, PTA has also been used for applications in additive manufacturing (AM) [13-15]. Conventionally, in AM, to deposit metallic powders layer by layer, high energy-density processes, such as laser or electron beam, are used. However, despite the high deposition speed and precision, they are not energetically efficient, creating demand for other methods. Arc processes, such as PTA, in this scenario, are candidates to provide the greater energy efficiency and higher deposition rates required, since the electron beam process has a deposition rate between 2 and 10 g/min, while arc processes range from 50 to 130 g/min [16]. Still, using nanoparticles in PTA can mitigate the epitaxial growth between the AM layers by favoring heterogeneous nucleation, which prevents a microstructure with preferential growth and, consequently, anisotropy in the manufactured component.

As nanoscale materials have a much larger surface area when compared to the same mass of larger scale materials, they have greater chemical reactivity and, consequently, offer special electrical and mechanical strength properties. Therefore, the insertion of nanoparticles is performed in order to improve the mechanical properties and the microstructure of the welded materials. The commonly employed nanoparticles in this case can be divided into two types: nanotubes and ceramic nanoparticles. Nanotubes, more specifically carbon nanotubes (CNTs), can be found as a cylinder of atoms organized in a single layer (Single-Walled Nanotubes) or in concentric cylinders (Multi-Walled Nanotubes) [2]. They are usually added to polymer matrices, but have already been used for the reinforcement of metallic matrices due to their properties. Experimental data show that the Young's modulus and yield point tend to increase with the amount of CNTs, as well as the hardness and the strain hardening [17]. However, applying large amounts of CNTs can degrade the properties of the material, due to their tendency to agglomerate [18].

Ceramic nanoparticles, on the other hand, including oxides, carbides and nitrides, with average sizes up to 100 nm, such as TiO<sub>2</sub>, TiC, WC and TiN, and have been used to reinforce metallic matrices. Many studies have observed that, in the presence of nanoceramics, the tensile strength, the impact, corrosion and wear resistance, as well as the yield point and the hardness limit are increased, and stable and refined microstructures are obtained [19-27].

The method to insert the nanoparticles into the metallic matrix matters, since, because of their high reactivity, they must be stopped from agglomerating. To enable the use as filler materials for welding, several methods were used to obtain homogeneous nanocomposites, such as: ARB (accumulative roll bonding), which impregnates nano-TiC in overlapping aluminum sheets for later lamination to obtain wires for the GTAW process [28]; ultrasonic stirring, which impregnated nano-WC in Ni/WC powder [25], and nano-TiC in Co superalloy powders (Stellite 6 and Stellite 12) for PTA; high speed ball mill to mix Stellite 6 nanoceramics for laser deposition [29]; ZrO<sub>2</sub> nanoparticles mixed in cellulose-coated electrode coatings [30]. Furthermore, the NPs can be inserted into a solution to be deposited on top of the sheet to be welded. This technique allows to increase the welding speed for the same laser power, since it increases its absorption coefficient, as did [31] apud [32].

In that context, this study presents a brief overview about the influence of ceramic nanoparticles in welding and adds to the step that comes before the welding deposition of powder filler materials. This work aims to insert, using the colloidal processing technique, ceramic nanoparticles (ZrO<sub>2</sub>) in a Co-based superalloy (Stellite 6), and analyze this nanocomposite's solidification event.

## 2. Materials and Methods

To study the influence of nanoparticles on the welding solidification structure, zirconia nanoparticles were inserted, through Fe-matrix carriers, into Co-based powder (Stellite 6) for later melting by PTA (plasma transferred arc).

The Fe-ZrO<sub>2</sub> carriers were prepared using colloidal processing technique [33]. The used metallic powder was iron (Diafe 2000, Dr. Fritsch Germany), which was characterized by particle size distribution, using the laser diffraction technique (Mastersizer, Malvern, United Kingdom); specific area using the BET method (Monosorb, MS-13, Quantachrome, USA) and density using He pycnometry (Monosorb Multipycnometer, Quantachrome, USA). The used colloidal zirconia, MELox Nanosize Undoped (Y<sub>2</sub>O<sub>3</sub>), was 5.5% volume or 25% weight of solids, according to the manufacturer, Mel Chemicals. Table 1 presents the properties of the iron powder and colloidal zirconia.

**Table 1.** Properties of the iron powder and colloidal zirconia.

Properties	Iron powder Fe-Diafe 200	Colloidal ZrO <sub>2</sub> MELox Nanosize
Particle size	1.63 (µm)	50 (nm)
Specific area (m <sup>2</sup> /g)	1.0	85-95
Density (g/cm <sup>3</sup> )	7.6	-

Ammonium polyacrylate (PAA, Duramax D3005, Rohm & Haas USA) was used as a dispersing agent, which helped maintain the pH of the suspension (alkaline). The carriers' preparation sequence started by inserting the dispersant in deionized water, followed by slowly adding iron powder, using a propeller stirrer for homogenization. This mixture ran through a ball mill for 1 h, in order to obtain an aqueous metallic suspension. Ceramic nanoparticles were added to the suspension, using 1 min of ultrasonic stirring, with the intent to disperse them in the metallic suspension. After the stabilization of each mixture, the aqueous part of the suspension was separated through drainage in plaster molds, previously dried in an oven, generating cast samples. In all prepared suspensions, the total of solids was 40% (in vol.), with 1, 2.5 and 7.5% of zirconia, and the remaining of Fe (39 and 37.5 and 32.5%, respectively). The resulting solid part makes the Fe-ZrO<sub>2</sub> carrier in enough amount to be added to the Co superalloy. Figure 1 shows, schematically, the carriers' preparation sequence.

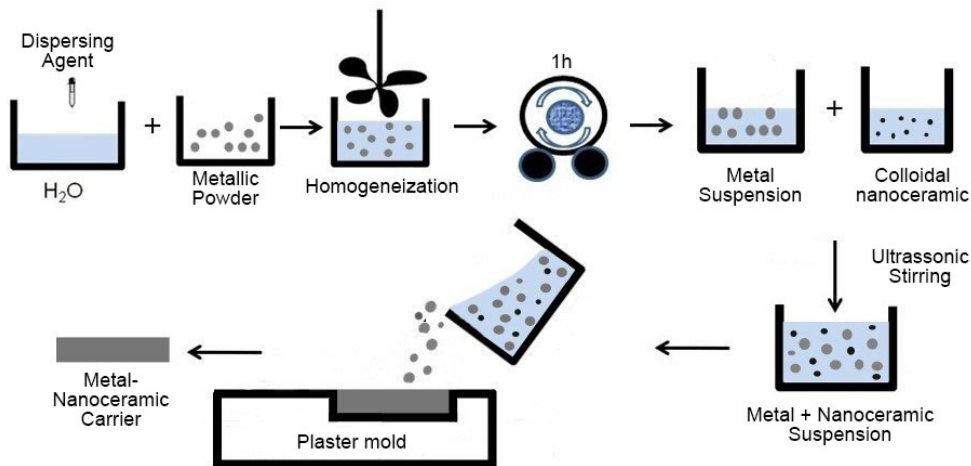


Figure 1. Schematic drawing of carrier preparation.

A Y-model powder mixer was used for a period of 45 min to mix/homogenize the Fe-ZrO<sub>2</sub> carriers in Stellite 6 powder (chemical composition on Table 2). The superalloy powder is spherical with granulometry mostly between 60 and 120µm. Four filler materials were produced: Stellite 6 with 1% Fe-ZrO<sub>2</sub> carrier, with increasing levels of zirconia (1, 2.5 and 7.5% volume) and Stellite 6 without any added zirconia, called St 6+ 1%; St 6 + 2.5%; St 6 + 7.5%; and St 6, respectively.

Table 2. Nominal chemical composition (weight percentage) of the Co superalloy (Stellite 6).

	Co	Cr	W	C	Ni	Mo	Fe	Si	Others
Nominal*	Balance	28.5	4.6	1.2	< 2.0	< 1.0	< 2.0	< 2.0	< 1.0
RXF**	59.075	32.582	4.6	NA	NA	0.67	2.133	NA	NA

\* [12]. \*\*The Stellite 6 powder was characterized by X-Ray Fluorescence (RFX).

From each powder mixture, 3 samples with 5g each were compacted into a cylindrical shape and subsequently fused with a plasma transferred arc welding source (PTA) (Figure 2) according to the parameters in Table 3. To avoid dilution, a copper base (100 x 75 x 12.5 mm) was used.

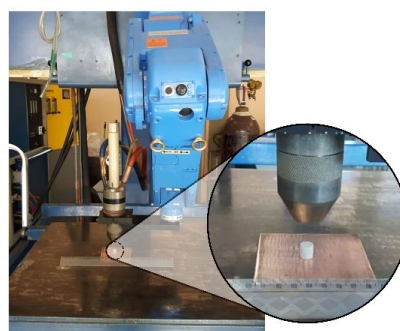


Figure 2. Cylindrical sample compacted with 5g of Stellite 6 with 1% carrier (Fe-ZrO<sub>2</sub>) over copper plate for later melting by PTA.

**Table 3.** PTA parameters.

CTWD (mm)	Plasma Gas (l/min)	Carrier Gas (l/min)	Gas Protection (l/min)	I (A)	Open electric arc time (s)
10	2	0.8	15	180	10

The fused samples were transversely cut, then embedded, then submitted to metallographic preparation including sanding with 120 to 600 grit silicon carbide sandpaper, followed by polishing with 1 and 3  $\mu\text{m}$  diamond paste. The microstructure was revealed with a concentrated hydrochloric acid +  $\text{Cr}_2\text{O}_3$  solution, submitted to electrolytic attack (1.5 V). The samples were analyzed from their cross sections with optical and scanning electron microscopy with field emission (SEM-FEG) and Vickers microhardness (HV 0.25). The phases were characterized by means of X-Ray Diffraction (XRD) with a Cu tube with  $2\theta$  ranging from 0 to  $90^\circ$  with a speed of  $0.5^\circ/\text{min}$ . The interdendritic spacing ( $\lambda$ ) was measured using the intersections method D, according to Equation 1.

$$\lambda = L / N - 1 \quad (1)$$

This method considers the total length of the primary dendritic arm, measured as L (with an average value of  $108.65 \mu\text{m} \pm 44.14$ ), and the number of secondary arms, N (with an average value of  $19 \pm 7$ ), counted only along one side of the primary arm. The final result ( $\lambda$ ) was determined from the average of 10 measurements according to the standard procedure reported in the literature [34,35].

In order to verify any significant measurement differences, one-way variance analysis (ANOVA) was used, with a 95% confidence interval, and Tukey's test with a significance level of 0.05 ( $p \leq 0.05$ ) [36].

### 3. Results

#### 3.1 Fe-ZrO<sub>2</sub> carriers

The dispersion of iron particles in an aqueous medium is one of the most critical stages of the colloidal process, since the preparation of a deflocculated suspension will lead to a better degree of particle packaging during the green forming phase.

The iron reactivity is directly linked to the metal/medium interface. Lussoli [37] evaluated the interfaces resulting from reactions in the Fe-H<sub>2</sub>O system and found hydroxyl ions ( $\text{OH}^-$ ), which, along with  $\text{Fe}^{+2}$ , could form ferrous hydroxide ( $\text{Fe}(\text{OH})_2$ ). That alkaline precipitate can have two important functions: (i) be the responsible agent to increase the pH (of the iron suspension) and (ii) act as a metal surface reactivity inhibitor, especially under high concentrations of these species. The latter contributed to control the iron's high reactivity, favoring a suspension with high concentrations of solids (40% vol.).

However, the presence of dispersing agents is essential, aiming at greater suspension stability and high fluidity, to be poured into a plaster mold. Adding such agent should provide a good coverage of the solid surface, thus preventing them from touching (Figure 3), which would favor agglomeration and sedimentation. In that regard, the PAA dispersant, due to the positive (ammonia) and negative (polyacrylate) parts, promoted the electrostatic effect, as well as the steric stabilization due to its long carbon chain, hindering the approximation between the particles.

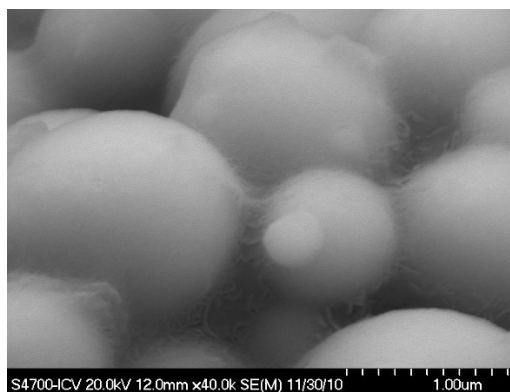


**Figure 3.** Dispersant action, covering metal particles.

Taking the iron suspension as a reference, previously prepared in the ball mill, different amounts of nanometric zirconia were added. However, the replacement of a fraction of micrometric iron particles with second-phase particles of nanometric size generated a bimodal size distribution, favoring the fluidity of the Fe-nanoceramic suspension [33]. Figure 4 shows details of such nanometric zirconia particles adsorbed on micrometric iron spheres bimodal system, called Fe-ZrO<sub>2</sub> carriers. When the number of ceramic nanoparticles is increased, the separation between them is reduced and, consequently, the interactions become stronger. That contributes to a greater particle aggregation (Figure 4: 7.5%). Still, in all amounts of zirconia, highly fluid suspensions were obtained to be manipulated via colloidal processing.

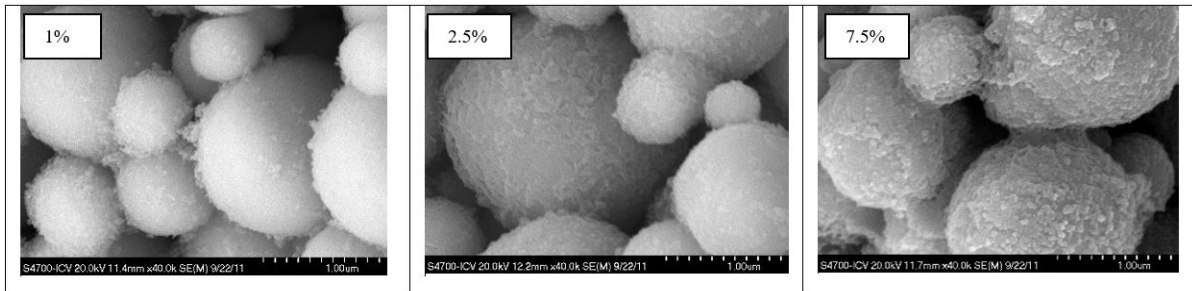


Figure 4. Fe-ZrO<sub>2</sub> carriers: increasing amounts of added zirconia (1, 2.5 and 7.5%) adsorbed onto spherical iron surfaces (FEG micrographs) [38].

So that the nanoparticle carriers (with a particle size of approximately 2 µm) can be used as a filler material in a welding process such as PTA, they must be mixed into a powder with a larger particle size (approximately 100 µm). Such particle size allows the powder to be moved by the carrier gas inside the nozzle until it reaches the plasma arc or the molten pool, depending on the nozzle's angle of convergence.

### 3.2 Mixture of Stellite 6 with Nano-ZrO<sub>2</sub> carriers after melting

Figure 5 shows the optical micrograph of the molten Stellite 6 alloy. A solidification structure is observed with dendrites of a Co-rich matrix ( $\alpha$ ) and a carbide interdendritic region ( $\alpha$  and carbides). Chrome (M<sub>7</sub>C<sub>3</sub>) carbide is the predominant form in that structure; Tungsten (M<sub>6</sub>C) carbide or Chrome (M<sub>23</sub>C<sub>6</sub>) carbide with poorer Carbon might have formed [11]. There are two different morphologies of Cr-carbides, namely blocky and radiated [39].

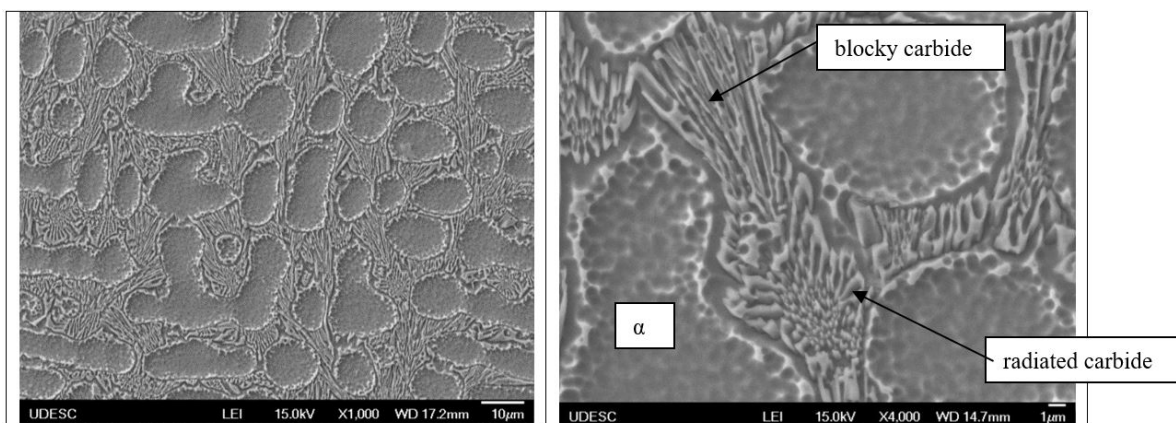


Figure 5. Molten Stellite 6 microstructure: dendrites of a Co-rich matrix ( $\alpha$ ) and a carbide interdendritic region ( $\alpha$  and carbides).

To evaluate the phases found in the material with and without adding the ZrO<sub>2</sub> nanoparticles, an XRD analysis was performed, Figure 6. The results show that the phases identified in Stellite 6 are: Co-rich solid solution with face-centered cubic and hexagonal systems, with carbides of Cr (Cr<sub>7</sub>C<sub>3</sub>) and Cr<sub>23</sub>C<sub>3</sub> and W (W<sub>2</sub>C).

Those phases remain at the same 2 $\theta$  angle in the other samples, therefore, showing no change in the crystalline structure due to the insertion of the ZrO<sub>2</sub> nanoparticles (Figure 6). The same behavior was observed by [40], who added TiC nanoparticles to Stellite 6. The ZrO<sub>2</sub> nanoparticles did not show in the diffractograms, because the XRD technique does not detect small amounts in the analyzed material.

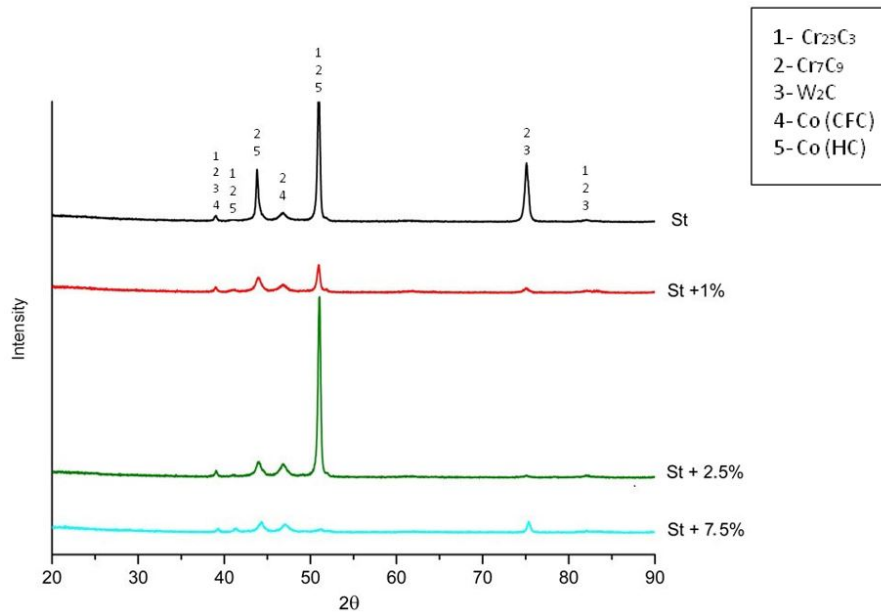


Figure 6. Comparison between the diffractograms of Stellite 6 without and with increasing amounts of added ZrO<sub>2</sub>.

The material's microstructure is refined, without porosity, due to the high cooling rate imposed by the PTA melting process, combined with the fast heat removal by the Cu substrate for all samples. The mean interdendritic space ( $\lambda$ ) is shown in Figure 7 and the detailed data in Table 4. The analysis shows that adding nanoparticles to Stellite 6 reduces the interdendritic spacing, especially in the case of adding of 1% ZrO<sub>2</sub>.

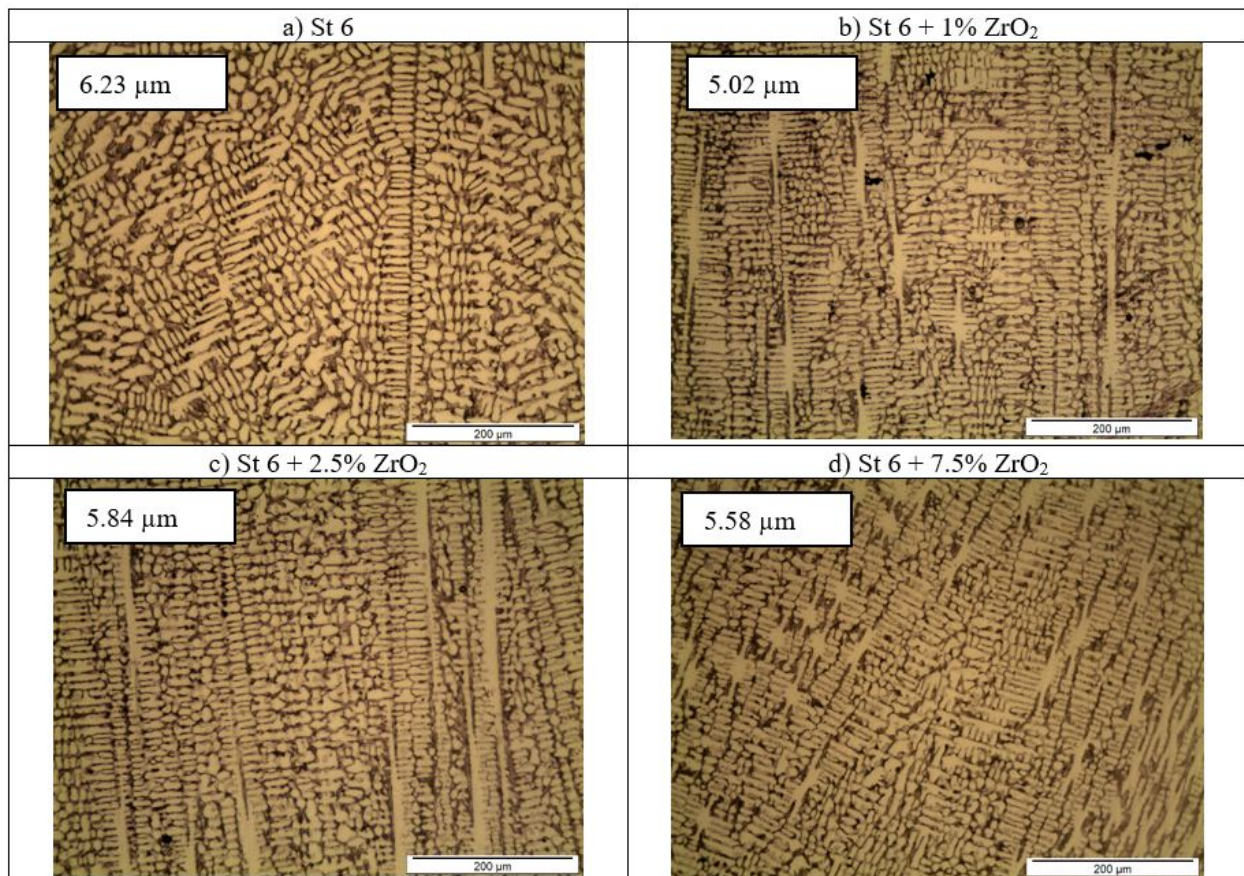


Figure 7. Microstructures of the molten samples: (a) Stellite 6 without and with added Fe carriers with (b) 1%, (c) 2.5%, (d) 7.5% ZrO<sub>2</sub>.

**Table 4.** Summary of interdendritic spacing data ( $\mu\text{m}$ ).

Group	Quantity*	Sum	Mean	Variance
St 6	10	62.33	6.23	1.32
St 6 + 1%	10	50.19	5.02	0.13
St 6 + 2.5%	10	58.45	5.84	0.41
St 6 + 7.5%	10	55.80	5.58	0.52

\*Number of primary dendrites measured per sample.

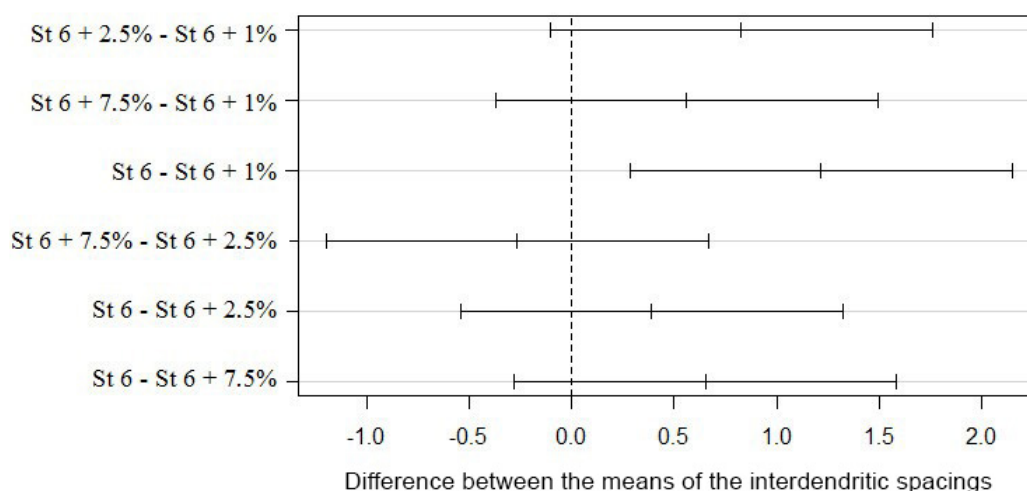
However, detailing the effect of the nanoparticles amount requires a more detailed analysis, with the aid of statistical tools. The statistical analysis through variance analysis (ANOVA), Table 5, proves that there are significant differences between the interdendritic spacing of the 04 types of materials, because the P-value is lower than the adopted 5%  $\alpha$  (significance value). The result confirms that adding nanoparticles impacts the microstructure refinement.

**Table 5.** Variance analysis of the mean interdendritic spacing in the cross section of the molten samples.

Source of Variation	SS	DoF	MS	F	P-value	Critical F
Between groups	7.800662	3	2.600221	<b>4.345266</b>	0.010333	<b>2.866266</b>
Within groups	21.54251	36	0.598403			
Total	29.34318	39				

Observation: Source of variation: zirconia concentration factor; SS: sum of squares; DoF: degrees of freedom; F: statistical F, ratio of the variance between samples by the variance within samples; P-value: probability of test significance; Critical F: it is a point on the test statistical distribution under the null hypothesis, it defines a set of values to reject the null hypothesis.

After statistically verifying a significant difference between the means of the interdendritic spacing values, a deeper analysis was performed using the Tukey multiple comparison test, and the results are shown in Figure 8. The significant difference is found in the comparison between the Stellite 6 and the Stellite 6 with added 1%  $\text{ZrO}_2$  samples. The difference between the St 6 and the St 6 + 1% means is never zero, that is, the means are never the same, leading to the conclusion that there is a difference between them.

**Figure 8.** Multiple Tukey comparisons for interdendritic spacing in the cross section of the molten samples.

Once there are significant differences between the interdendritic spacings of the St 6 and St 6 + 1% samples, a chemical analysis was performed using EDS/FEG (Figure 9). This specific EDS analysis of the molten Stellite 6 samples without added nanoparticles showed two types of carbides in the interdendritic space: dark  $\text{M}_7\text{C}_9$  and/or  $\text{M}_{23}\text{C}_3$  (Cr) in lamellar form, and light  $\text{M}_2\text{C}$  (W) dispersed according to the literature [41]. Adding Fe carriers with 1%  $\text{ZrO}_2$  nanoparticles did not change the type of carbides produced during solidification. However, higher levels of Fe were found. As reported by [42], the increase in Fe content decreased the amount of Co elements in dendritic regions.

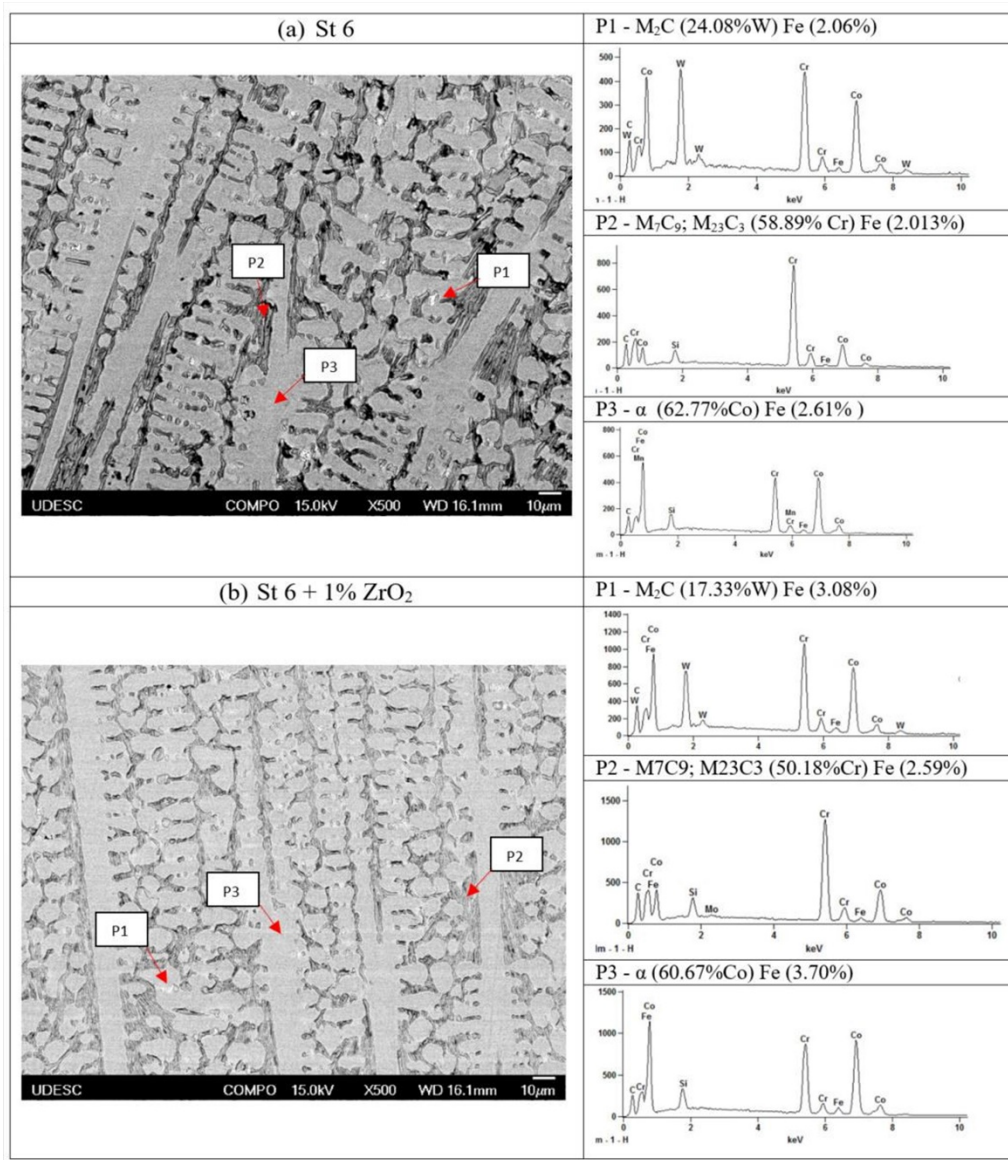


Figure 9. Specific EDS microstructure analysis: (a) Stellite 6 and (b) Stellite 6 with added Fe carriers with 1%  $ZrO_2$  nanoparticles.

The impact of adding nanoparticles was also evaluated from the microhardness of the molten samples, and the results are shown in Figure 10. The samples were melted on copper plates, thus avoiding dilution of the base metal in the molten pool. In the cobalt superalloy system (Stellite 6), the added Fe turns the compositions more hypoeutectic, resulting in a reduction in hardness [43,44] which can mitigate the impact of the added ceramic nanoparticles. Besides, to limit the number of variables influencing the results, the same melting parameters (open arc time and current intensity) were used for all tested compositions.

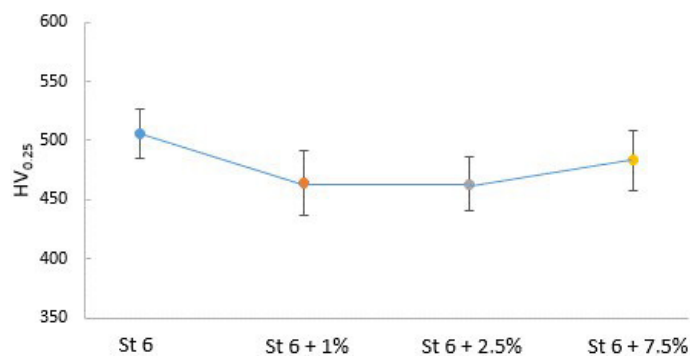


Figure 10. Microhardness of molten Stellite 6 samples without and with increasing amounts of added nano  $ZrO_2$ .

The microhardness values of Stellite 6 (without added nanoparticles) are in the range of 500 HV, a result consistent with that obtained by [45], who evaluated the Stellite 6 deposited by PTA on a Cu substrate (without dilution with the base material). Despite the previously observed greater microstructure refinement, the added nanoparticles brought about a tendency of microhardness reduction. As the number of nanoparticles increases, the hardness tends to increase as well, while still staying lower than that of the Co alloy without the added nanoparticle carriers.

#### 4. Discussion

Nanoparticles are usually added to welding filler materials to improve mechanical properties (increasing hardness, tensile strength and impact properties). Such improvements can be correlated to an increase in acicular ferrite content, grain refinement, more homogeneous distribution of hard nanoparticles as a matrix reinforcement. In this context, some papers stand out to show how ceramic nanoparticles influence welds.

Including nano-TiO<sub>2</sub> in the coating of electrodes for welding C steels increases the amount of acicular ferrite in the weld microstructure, due to an increased amount of complex inclusions of Mn-Ti oxides, from which acicular ferrite nucleates; and to the adhesion of nano oxides to the grain boundaries that prevents the growth of allotropomorphic ferrite and Widmanstatten patterns. The increase in nucleation, as well as the anchoring of grain boundaries, ensures, in those cases, a more refined microstructure, directly improving the mechanical properties of the material [17,18]. Pal and Maity [23] also state that the inclusion of nano TiO<sub>2</sub> induces the recovery of some chemical elements such as Mn, Ni, Mo, promoting an increase in complex inclusions.

The increase in weld hardness can be correlated to the refinement of the microstructure, as well as to the homogeneous distribution of hard particles in the matrix. In the study carried out by [19] with the addition of nano TiC in wires for TIG welding in Al, besides the same previously-mentioned effect for steels (increase in nucleation and anchoring of grain boundaries) refining the grain size of the  $\alpha$ -Al phase, TiC nanoparticles reinforce the Al matrix. Due to differences in the thermal expansion coefficients, plastic deformation fields are formed around the nanoparticles, leading to a hardening of the matrix. The same behavior was reported by [26], who added nano-WC and La<sub>2</sub>O<sub>3</sub> to reinforce carbon steel laser-deposited WC/Ni coatings. Adding those elements increased coating homogeneity, microstructure refinement and hardness, mainly with nano-WC. Besides increasing hardness, adding nanoparticles increased resistance to corrosion and wear [27]. Molina-Claros et al. [25] highlight the behavior of cracks, which were reduced with the inclusion of nano-WC in a WC/Ni alloy deposited by PTA in carbon steel. They were found to spread more easily in regions without WC. However, in the presence of WC nanoparticles, those regions were reduced due to viscosity changes in the molten pool, restricting the cracks to a small surface portion of the weld bead.

In PTA-processed coatings, incorporating refractory nanoceramics in cobalt alloys, such as TiC, does not aim to change the matrix crystalline structure, but rather to act on the phase nucleation stage and the anchoring of dislocations. As a nucleating agent, they reduce the size of phases such as Co<sub>6</sub>W<sub>6</sub>C, Co<sub>3</sub>W<sub>3</sub>C, which are formed due to the dilution of the WC particles, or FeW<sub>3</sub>C and Fe<sub>3</sub>W<sub>3</sub>C, in case the ceramic nanoparticle insertion system presents the iron element [40].

In this context, adding ZrO<sub>2</sub> nanoparticles to a Co-based matrix was expected to increase hardness due to the microstructure refinement, as well as to the distribution of hard monoclinic zirconia particles, 1530 HV [46], in the cobalt superalloy matrix, with an average hardness of 500 HV [45]. However, the hardness levels decreased (Figure 10), which can be attributed to an increase in Fe in the Stellite 6 chemical composition. This chemical element should be limited to 2% according to its nominal composition (Table 1). However, the carrier produced by the colloidal processing technique has an expressive amount of Fe, since it corresponds, in volume, to 99% of the Fe-ZrO<sub>2</sub> (1% of nanoparticle). Previous results [43,44] show that an increase in the Stellite 6 alloy Fe content yields a reduction in the amount of eutectic carbides and increases the volumetric fraction of the Co-rich solid solution formed during solidification, decreasing the final hardness of the material. The results suggest that such behavior prevails over the refinement occurred in the molten microstructure. According to the performed statistical analysis, the microstructure refinement was significant for samples with 1% zirconia, however the literature does not quantify the expected refinement with the added nanoparticles. Several studies point out that, if the insertion of nanoparticles exceeds a certain threshold, properties may deteriorate, the exact opposite of what is sought with their addition [10,21,24-27]. Thus, besides to the Fe content effect, the appropriate amount of nanoparticles to be incorporated into the filler material must be considered to keep a positive influence on the mechanical properties, which was found to be 1% zirconia in this study.

#### 5. Conclusion

Producing iron suspensions in an aqueous medium with up to 40% of solids and zirconia nanoparticles, called Fe-ZrO<sub>2</sub> carriers, is possible using the colloidal processing technique. The carriers were proven suitable for insertion into Co-based superalloys with grain sizes compatible with the PTA welding process, which suggests that they can be used in depositing nanostructured coatings, as well as in the development of additive manufacturing techniques with arc welding. Under this work's conditions, the interdendritic spacing significantly decreased with the addition of Fe carriers with 1% ZrO<sub>2</sub> in Stellite 6, which did not take place when higher amounts of zirconia were added. Contrary to expectations, such refinement did not increase the

hardness of the molten microstructure. The Fe content added by the carriers is believed to be responsible for the reduction in the levels of that property.

## References

- [1] Morris J, Willis JUS. Environmental protection agency nanotechnology white paper. Washington: U.S. Environmental Protection Agency; 2007.
- [2] Aitken RJ, Chaudhry MQ, Boxall AB, Hull M. Manufacture and use of nanomaterials: Current status in the UK and global trends. *Occupational Medicine*. 2006;56(5):300-306. <http://dx.doi.org/10.1093/occmed/kql051>. PMID:16868127.
- [3] Nowack B, Bucheli TD. Occurrence, behavior and effects of nanoparticles in the environment. *Environmental Pollution*. 2007;150(1):5-22. <http://dx.doi.org/10.1016/j.envpol.2007.06.006>. PMID:17658673.
- [4] Buzea C, Pacheco II, Robbie K. Nanomaterials and nanoparticles: sources and toxicity. *Biointerphases*. 2007;2(4):MR17-MR71. <http://dx.doi.org/10.1116/1.2815690>. PMID:20419892.
- [5] Moreno R. *Reología de suspensiones cerámicas*. Madrid: Consejo Superior de Investigaciones Científicas; 2005.
- [6] Vieira Junior LE, Bendo T, Nieto MI, Klein AN, Hotza D, Moreno R, et al. Processing of copper based foil hardened with zirconia by non-deformation method. *Materials Research*. 2017;20(3):835-842. <http://dx.doi.org/10.1590/1980-5373-mr-2016-0574>.
- [7] Burgos-Montes O, Moreno R. Stability of concentrated suspensions of Al<sub>2</sub>O<sub>3</sub>-SiO<sub>2</sub> measured by multiple light scattering. *Journal of the European Ceramic Society*. 2009;29(4):603-610. <http://dx.doi.org/10.1016/j.jeurceramsoc.2008.07.044>.
- [8] Gillani S, Mir S, Masood M, Khan AK, Rashid R, Azhar S, et al. Triple-component nanocomposite films prepared using a casting method: Its potential in drug delivery. *Journal of Food and Drug Analysis*. 2017;26(2):887-902. <http://dx.doi.org/10.1016/j.jfda.2017.02.006>.
- [9] Venet M, Santa-Rosa W, M'Peko J-C, Amorín H, Algueró M, Moreno R. Controlling colloidal processing of (K, Na) NbO<sub>3</sub>-based materials in aqueous medium. *Journal of the European Ceramic Society*. 2019;39(12):3456-3461. <http://dx.doi.org/10.1016/j.jeurceramsoc.2019.02.026>.
- [10] Harichandran R, Selvakumar N. Effect of nano/micro B<sub>4</sub>C particles on the mechanical properties of aluminium metal matrix composites fabricated by ultrasonic cavitation-assisted solidification process. *Archives of Civil and Mechanical Engineering*. 2016;16(1):147-158. <http://dx.doi.org/10.1016/j.acme.2015.07.001>.
- [11] Davis JR. *Hardfacing, weld cladding and dissimilar metal joining*. Vol. 6. New York: ASM International; 1993.
- [12] Kennametal Stellite. *Apresenta as características de seus produtos*. Pittsburgh: Kennametal Stellite; 2019. [acesso em 1 jun. 2016]. Disponível em: <http://www.stellite.com/>
- [13] Cardozo EP, Pardal GR, Ríos S, Ganguly S, D'Oliveira ASCM. Additive techniques to refurbish Ni Based Components. *Soldagem e Inspeção*. 2019;24(0):1-11. <http://dx.doi.org/10.1590/0104-9224/si24.03>.
- [14] Alberti EA, Bueno BMP, D'Oliveira ASCM. Additive manufacturing using plasma transferred arc. *International Journal of Advanced Manufacturing Technology*. 2016;83(9-12):1861-1871. <http://dx.doi.org/10.1007/s00170-015-7697-7>.
- [15] Cardozo EP, Ríos S, Ganguly S, D'Oliveira ASCM. Correction to: Assessment of the effect of different forms of Inconel 625 alloy feedstock in Plasma Transferred Arc (PTA) additive manufacturing. *International Journal of Advanced Manufacturing Technology*. 2018;98(5-8):1707. <http://dx.doi.org/10.1007/s00170-018-2394-y>.
- [16] Alberti EA, Silva LJ, D'Oliveira ASCM. Manufatura Aditiva: O papel da soldagem nesta janela de oportunidade. *Soldagem e Inspeção*. 2014;19(2):190-198. <http://dx.doi.org/10.1590/0104-9224/Si1902.11>.
- [17] Bhat A, Balla VK, Bysakh S, Basu D, Bose S, Bandyopadhyay A. Carbon nanotube reinforced Cu-10Sn alloy composites: mechanical and thermal properties. *Materials Science and Engineering A*. 2011;528(22):6727-6732. <http://dx.doi.org/10.1016/j.msea.2011.05.038>.
- [18] Bakshi SR, Lahiri D, Agarwal A. Carbon nanotube reinforced metal matrix composites - A review. *International Materials Reviews*. 2010;55(1):41-64. <http://dx.doi.org/10.1179/095066009X12572530170543>.
- [19] Fattahi M, Mohammady M, Sajjadi N, Honarmand M, Fattahi Y, Akhavan S. Effect of TiC nanoparticles on the microstructure and mechanical properties of gas tungsten arc welded aluminum joints. *Journal of Materials Processing Technology*. 2015;217:21-29. <http://dx.doi.org/10.1016/j.jmatprotec.2014.10.023>.
- [20] Fattahi M, Nabhani N, Hosseini M, Arabian N, Rahimi E. Effect of Ti-containing inclusions on the nucleation of acicular ferrite and mechanical properties of multipass weld metals. *Micron*. 2013;45:107-114. <http://dx.doi.org/10.1016/j.micron.2012.11.004>. PMID:23238108.
- [21] Fattahi M, Nabhani N, Vaezi MR, Rahimi E. Improvement of impact toughness of AWS E6010 weld metal by adding TiO<sub>2</sub> nanoparticles to the electrode coating. *Materials Science and Engineering A*. 2011;528(27):8031-8039. <http://dx.doi.org/10.1016/j.msea.2011.07.035>.
- [22] Orishich AM, Malikov AG, Cherepanov AN. Effect of nanopowder modifiers on properties of metal laser-welded joints. *Physics Procedia*. 2014;56:507-514. <http://dx.doi.org/10.1016/j.phpro.2014.08.005>.

- [23] Pal TK, Maity UK. Effect of nano size TiO<sub>2</sub> particles on mechanical properties of AWS E 11018M type electrode. *Materials Sciences and Applications*. 2011;2(9):1285-1292. <http://dx.doi.org/10.4236/msa.2011.29173>.
- [24] Vimalraj C, Kah P, Belinga EM, Martikainen J. Effect of nanomaterial addition using GMAW and GTAW processes. *Reviews on Advanced Materials Science*. 2016;44:370-382.
- [25] Molina-Claros J, Hdz-García HM, Alvarez-Vera M, Pech-Canul MI, Muñoz-Arroyo R, García-Vázquez F, et al. Characterization of PTA processed overlays without and with WC nanoparticles. *Surface Engineering*. 2017;33(11):857-865. <http://dx.doi.org/10.1080/02670844.2017.1323442>.
- [26] Farahmand P, Liu S, Zhang Z, Kovacevic R. Laser cladding assisted by induction heating of Ni-WC composite enhanced by nano-WC and La<sub>2</sub>O<sub>3</sub>. *Ceramics International*. 2014;40(10):15421-15438. <http://dx.doi.org/10.1016/j.ceramint.2014.06.097>.
- [27] Farahmand P, Kovacevic R. Corrosion and wear behavior of laser clad Ni-WC coatings. *Surface and Coatings Technology*. 2015;276:121-135. <http://dx.doi.org/10.1016/j.surfcoat.2015.06.039>.
- [28] Sokolov GN, Zorin IV, Artem'ev AA, Litvinenko-Ar'kov VB, Dubtsov YN, Lysak VI, et al. Structure formation and properties of weld alloys with addition of refractory compound nanoparticles. *Inorganic Materials: Applied Research*. 2015;6(3):240-248. <http://dx.doi.org/10.1134/S2075113315030119>.
- [29] Montealegre MA, Pérez AT, Arias JL, Castro G, González M. Laser cladding of cobalt alloy with ceramic nanopowder on steel. In: *The Laser Institute. Proceedings of the 29th International Congress on Applications of Lasers & Electro-Optics, 2010; Cambridge*. Cambridge: LIA; 2010. p. 298-303. <http://dx.doi.org/10.2351/1.5062040>.
- [30] Dabiri AR, Yousefi Mojallal R, Ahmadi E, Fattahi M, Amir Khanlou S, Fattahi Y. Effect of ZrO<sub>2</sub> nanoparticles on the impact properties of shielded metal arc welds. *Materials Letters*. 2015;158:325-328. <http://dx.doi.org/10.1016/j.matlet.2015.05.159>.
- [31] Afonin YV, Cherepanov A, Orishich AM. Laser welding of titanium using nanopowder inoculants. In: *Proceedings of the 12nd Investigation, Development and Application of Advanced Technologies in Industry; 2008; St Peterburg*. St Peterburg: 2008. p. 322-324.
- [32] Kuznetsov MA, Zernin EA. Nanotechnologies and nanomaterials in welding production. *Welding International*. 2011;64(12):23-26.
- [33] Lussoli RJ, Rodrigues Neto JB, Klein AN, Hotza D, Moreno R. Aqueous colloidal processing of carriers for delivering silica nanoparticles in iron matrix nanocomposites. *Materials Research Bulletin*. 2013;48(7):2430-2436. <http://dx.doi.org/10.1016/j.materresbull.2013.02.010>.
- [34] Vandersluis E, Ravindran C. Comparison of measurement methods for secondary dendrite arm spacing. *Metallography, Microstructure, and Analysis*. 2017;6(1):89-94. <http://dx.doi.org/10.1007/s13632-016-0331-8>.
- [35] Iben Houria M, Nadot Y, Fathallah R, Roy M, Maijer DM. Influence of casting defect and SDAS on the multiaxial fatigue behavior of A356-T6 alloy including mean stress effect. *International Journal of Fatigue*. 2015;80:90-102. <http://dx.doi.org/10.1016/j.ijfatigue.2015.05.012>.
- [36] Devore JL. *Probabilidade e estatística para engenharia e ciências*. São Paulo: Pioneira Thomson Learning; 2006.
- [37] Lussoli RJ. *Desenvolvimento de portadores de nanopartículas cerâmicas como nucleante para solidificação de ferro fundido cinzento*. Florianópolis: UFSC; 2011.
- [38] Santos BC, Lussoli RJ, Rodrigues Neto JB, D'Oliveira ASCM, Bond D. Incorporação de nanopartículas cerâmicas em pós-metálicos para soldagem PTA. In: *Associação Brasileira de Soldagem. Anais do 42º Congresso Nacional de Soldagem; 2016; Belo Horizonte*. Belo Horizonte: ABS; 2016.
- [39] Hou QY, Gao JS, Zhou F. Microstructure and wear characteristics of cobalt-based alloy deposited by plasma transferred arc weld surfacing. *Surface and Coatings Technology*. 2005;194(2-3):238-243. <http://dx.doi.org/10.1016/j.surfcoat.2004.07.065>.
- [40] Acevedo-Dávila JL, Muñoz-Arroyo R, Hdz-García HM, Martínez-Enriquez AI, Alvarez-Vera M, Hernández-García FA. Cobalt-based PTA coatings, effects of addition of TiC nanoparticles. *Vacuum*. 2017;143:14-22. <http://dx.doi.org/10.1016/j.vacuum.2017.05.033>.
- [41] Klarstrom D, Crook P, Wu J. *Metallography and microstructures of cobalt and cobalt alloys*. Vol. 9. New York: ASM International; 2004.
- [42] Paes RMG, Scheid A. Effect of deposition current on microstructure and properties of CoCrWC alloy PTA coatings. *Soldagem e Inspeção*. 2014;19(3):247-254. <http://dx.doi.org/10.1590/0104-9224/S11903.07>.
- [43] Yaedu AE, D'Oliveira ASCM. Cobalt based alloy PTA hardfacing on different substrate steels. *Materials Science and Technology*. 2005;21(04):459-466. <http://dx.doi.org/10.1179/174328413X13789824293380>.
- [44] Ferozhkhan MM, Kumar KG, Ravibharath R. Metallurgical study of Stellite 6 cladding on 309-16L stainless steel. *Arabian Journal for Science and Engineering*. 2017;42(5):2067-2074. <http://dx.doi.org/10.1007/s13369-017-2457-7>.
- [45] Gomes RJN, Henke S, D'Oliveira ASCM. Microstructural control of Co-based PTA coatings. *Materials Research*. 2012;15(5):796-800. <http://dx.doi.org/10.1590/S1516-14392012005000099>.
- [46] Lucas TJ, Lawson NC, Janowski GM, Burgess JO. Effect of grain size on the monoclinic transformation, hardness, roughness, and modulus of aged partially stabilized zirconia. *Dental Materials*. 2015;31(12):1487-1492. <http://dx.doi.org/10.1016/j.dental.2015.09.014>. PMID:26490101.